Supplementary material for Kurz et al., Comparing cone-beam CT intensity correction methods for dose recalculation in adaptive intensity modulated photon and proton therapy for head and neck cancer, Acta Oncol, 2015; 54: 1651–1657.

Supplementary Table I. Overview of the investigated patient cohort.

Patient ID	Tumor site	TNM stage	$\Delta t_{rpCT\text{-}CBCT}$ (days)	Prescription low/high dose PTV (Gy)	Number of fractions	SFUD gantry angle (degree)
PatCA1	Larynx	pT2pN0M0	1	50/–	25	45
PatCA2	Hypopharynx, esophagus	cT4cN2M0	2	50.4/56	28	45
PatCA3	Larynx	pT1bN0M0	1	54/60	30	315
PatCA4	Hypopharynx	cT2cN2bM0	1	54/60	30	315
PatCA5	Nasopharynx	cT2cN2bM0	0	54/60	30	315
PatCA6	Larynx	pT2bpN1M0	3	50.4/56	28	45
PatCR1	Paranasal sinus	pT2cN0M0	1	50.4/61.6	28	270
PatCR2	Paranasal sinus	pT3N2bM0	0	54.4/64	32	0
PatCR3	Nasal cavity	cT3N0M0	1	50.4/56	28	90

For the nine investigated patients of this study, tumor site, TNM stage, dose prescription in the high and low dose PTV for the SIB treatment phase, number of SIB treatment fractions and time delay between rpCT and CBCT acquisition $\Delta t_{rpCT\text{-}CBCT}$ are given. The gantry angle of the generated SFUD plans is indicated, as well.

Supplementary Table II. OAR dose/volume constraints used during treatment planning.

	Dose/volume parameter	Tolerance dose (Gy)
Spinal cord	D_{max}	53
Brain stem	D_{max}	53
Parotids	D_{mean}	26
Optical nerves	D_{max}	54
Chiasm	D_{max}	56
Eyes	D_{max}	45
Eye lenses	D_{mean}	10

For the spinal cord, brain stem, optical nerves and chiasm, PRVs have been considered throughout this study. The optical nerves, chiasm, eyes and eye lenses constraints were only used for PatCR1–3, where these structures were delineated. The tolerance dose levels were chosen similar to the clinical values used for IMRT plan optimization at our institution.

Supplementary Table III. Gamma-index pass-rates for vCT- and $CBCT_{LUT}$-based dose recalculations.

	IMRT		IMPT	
	vCT (%)	$CBCT_{LUT}$ (%)	vCT (%)	$CBCT_{LUT}$ (%)
PatCA1	96	93	95	88
PatCA2	91	85	76	74
PatCA3	97	90	95	74
PatCA4	96	87	93	83
PatCA5	95	89	90	83
PatCA6	94	89	88	80
PatCR1	99	99	94	97
PatCR2	99	99	98	97
PatCR3	89	92	93	90

For each considered patient the vCT- and $CBCT_{LUT}$-based dose recalculation is compared to the rpCT-based recalculation by a (3%, 3 mm) 3D global gamma criterion.

Supplementary Table IV. BEV range pass-rates for vCT- and $CBCT_{LUT}$-based SFUD dose compared to the rpCT-based calculation.

	vCT (%)	$CBCT_{LUT}$ (%)
PatCA1	88	80
PatCA2	95	94
PatCA3	93	88
PatCA4	95	93
PatCA5	94	81
PatCA6	93	83
PatCR1	89	88
PatCR2	96	80
PatCR3	99	86

For each patient the vCT- and $CBCT_{LUT}$-based proton SFUD dose recalculation is compared to the rpCT-based recalculation in terms of the proton range in BEV. The depicted values indicate the amount of 1D profiles found within 3 mm of the rpCT.

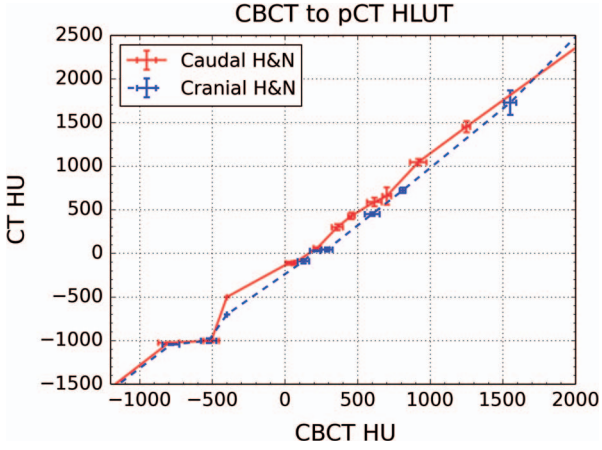

Supplementary Figure 1. HLUTs applied for intensity rescaling of the CBCT to the pCT. The two HLUTs used for patients with caudally (solid) and cranially located (dashed) lesions are depicted. Each data-point corresponds to a population average over multiple corresponding points in the registered pCT and CBCT in a narrow Hounsfield unit (HU) interval. The standard deviation at each point is indicated by error-bars.

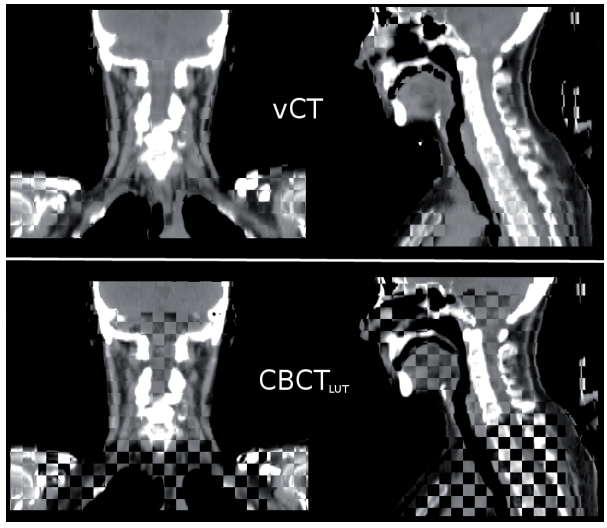

Supplementary Figure 2. Checkerboard display of vCT (upper row) and CBCT$_{LUT}$ (lower row) against the rpCT of PatCA2.

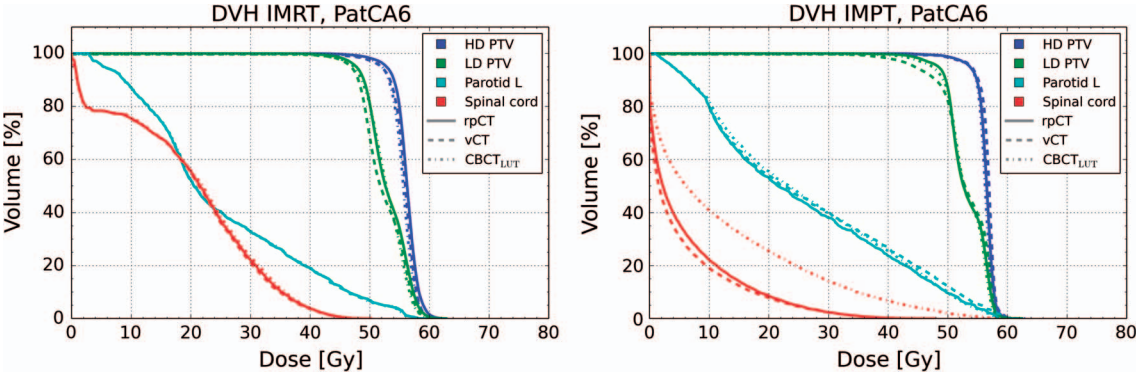

Supplementary Figure 3. DVH comparison of the IMRT (left) and IMPT (right) dose distributions of PatCA6 recalculated on the rpCT (solid line), vCT (dashed) and CBCT$_{LUT}$ (dotted). For improved visibility, only the high (HD) and low dose (LD) PTV (blue and green), as well as the left parotid (cyan) and the spinal cord (red) are depicted.

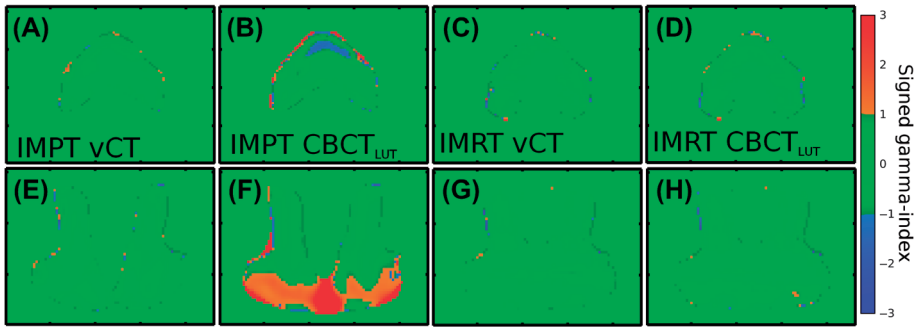

Supplementary Figure 4. Signed gamma-index displayed in a central axial (top row, A–D) and coronal slice (bottom row, E–H) for PatCA3. IMPT recalculations using the vCT (left column, A, E) and CBCT$_{LUT}$ (center-left column, B, F), as well as IMRT recalculations using the vCT (center-right column, C, G) and CBCT$_{LUT}$ (right column, D, H) are compared to the corresponding rpCT dose distribution.